

Restrictions of microwave electrometry due to nonlocal interactions in Rydberg atoms

Bin-Bin Wang, Xiao-Jun Zhang, and Jin-Hui Wu^{✉*}

Center for Quantum Sciences and School of Physics, Northeast Normal University, Changchun 130117, People's Republic of China

(Received 21 March 2024; revised 9 June 2024; accepted 26 July 2024; published 12 August 2024)

Large dipole moments between high Rydberg states have been utilized to measure microwave electric fields based on electromagnetically induced transparency, while nonlocal Rydberg interactions are not suitably addressed yet in most relevant works. Here we adopt a mean-field superatom model to investigate the main restrictions of Rydberg microwave electrometry due to nonlocal interactions in atomic samples of appropriate densities. It is found that accurate microwave measurements can be attained in the linear regime only for dilute enough atomic samples and not too strong probe fields, which jointly determine whether Rydberg excitations are insignificant. This then leads to the critical lines of atomic density and probe intensity, below which the discrepancy between measured and real values is negligible due to vanishing Rydberg interactions, for a fixed microwave or coupling field. Our findings are instructive to identify the optimal conditions for Rydberg microwave electrometry by reaching a compromise between high precisions and high accuracies, requiring, respectively, large and small numbers of Rydberg excitations, when measuring weaker microwave fields.

DOI: 10.1103/PhysRevApplied.22.024034

I. INTRODUCTION

Rydberg atoms [1] refer to atoms in highly excited states with large principal quantum numbers ($n \gg 1$), hence exhibiting very large atomic radii ($\propto n^2$, up to μm) and very long radiative lifetimes ($\propto n^3$, up to 100 μs). It is more useful to note that very large dipole moments ($\propto n^2$, of the order of $10^3 ea_0$) can be found between densely distributed Rydberg states with widely selectable energy spacings ($\propto n^{-3}$, covering most microwave frequencies). These distinctive features make high-lying Rydberg atoms of great interest in the frontier fields of microwave measurement [2–22], quantum sensing [23–27], quantum imaging [28–32], etc. In particular, researchers have achieved remarkable successes in the sensitive microwave measurements using low-excitation-density Rydberg atomic gases [2–20] based on the quantum optical techniques of electromagnetically induced transparency (EIT) [33] and Autler-Towns (AT) splitting [34,35]. The amplitude and sensitivity of minimum detectable microwave electric field demonstrated in these experiments are significantly lower than those achieved using typical antenna-based methods [2,36] and can be further reduced by developing a superheterodyne receiver [7]. Moreover, antenna-based methods are subjected to limitations in terms of frequency range and calibration complexity since antennas will lead to perturbations of microwave electric fields and suffer from out-of-band interference

[30,36,37]. Rydberg-based microwave sensing, as an alternative approach, exhibits advantages such as direct SI unit calibration, wide bandwidth, compact size, and no metal disturbance [30] in addition to high sensitivity due to, e.g., the invariance of atomic intrinsic parameters and an up-converted readout from microwave amplitude to optical frequency.

So far, most researches focusing on the microwave electrometry based on Rydberg atomic gases are implemented at room temperature by taking the frequency interval between two transmission peaks in a Rydberg EIT-AT experiment as a direct measure of the microwave field. But, hot atoms will bring unexpected problems [2,37], such as Doppler broadening, atomic collision, black-body radiation, and transit time broadening, which must increase the linewidths of transmission peaks and hinder the measurement of weaker microwave fields. In contrast, cold atoms help to overcome these problems so that it is viable to improve the measurement accuracy [15,38] until approaching the standard quantum limit (SQL) [23,37] by increasing the number of Rydberg excitations [8,39]. This strategy is restricted however by another intrinsic feature of Rydberg atoms, nonlocal van der Waals (vdW) and dipole-dipole (DD) interactions, which are beneficial to the development of quantum memory, quantum computing, and quantum simulation [40–45] but become significant only for dense atomic samples and strong probe fields. Then, it is necessary to understand what are the roles of vdW and DD interactions in Rydberg microwave electrometry though, in most previous studies

*Contact author: jhwu@nenu.edu.cn

working with dilute atomic samples and weak probe fields [2,15,46], these interactions (about 100 Hz or smaller) have not been studied in depth. We only find in a recent experiment [8] that strong Rydberg interactions are explored to improve the sensing precision of microwave field by utilizing the enhanced sensitivity close to a critical transition point in a many-body nonlinear model. To the best of our knowledge, no works have been devoted to investigating the effects of weak Rydberg interactions in microwave electrometry, especially when they change gradually from vanishing to non-negligible.

In this work, we try to study the main effects of vdW and DD interactions on the microwave field measurement by considering a four-level cascade system of cold Rydberg atoms coherently driven by a probe, a coupling, and a microwave field. This is done by examining the AT split EIT spectra of the probe field by varying the microwave field as a mean-field superatom (SA) model [47–49] is adopted to treat the vdW and DD interactions in terms of energy shifts and coupling rates, respectively, with respect to two Rydberg states. Numerical results show that the linear regime where accurate microwave measurement can be achieved depends on both atomic density and probe intensity, and it is possible to work in this linear regime for a relatively large atomic density using a weak enough probe intensity. We also provide critical lines, manifested as the joint variations of atomic density and probe intensity, that can be chosen to accurately measure a certain microwave field for a fixed coupling field without being affected by Rydberg interactions. Finally, we present the amplitude and sensitivity of minimum detectable electric field restricted by Rydberg interactions.

We further explain our motivations as follows. In Rydberg microwave electrometry, dense atomic samples or strong probe fields are required to attain essential Rydberg excitations enabling high sensing precisions, while dilute atomic samples and weak probe fields are required to ensure negligible Rydberg interactions enabling high sensing accuracies. It is also desired to narrow down the transmission linewidth, facilitating the accurate sensing of weaker microwave fields, by increasing atomic density in the presence of negligible Rydberg interactions. Thus, it should be of interest to examine, in which regimes of atomic densities (or Rydberg excitations), one can reach the highest precisions yet without sacrificing too much accuracy by tuning the probe Rabi frequency.

II. MODEL AND EQUATIONS

We consider a four-level cascade system of cold atoms with three transitions $|1\rangle \leftrightarrow |2\rangle$, $|2\rangle \leftrightarrow |3\rangle$, and $|3\rangle \leftrightarrow |4\rangle$ driven by a probe field of frequency (amplitude) ω_p (E_p), a coupling field of frequency (amplitude) ω_c (E_c), and a microwave field of frequency (amplitude) ω_m (E_m), respectively, as shown in Fig. 1(a). Corresponding

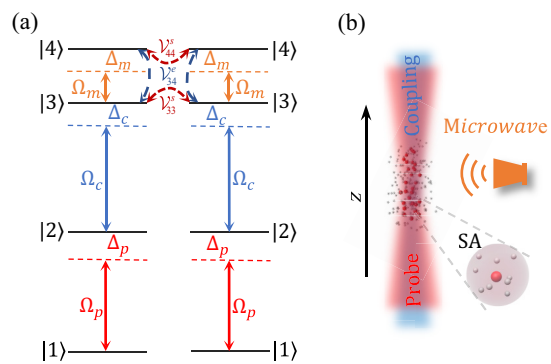


FIG. 1. (a) Configuration of a four-level atomic system driven by a probe field on transition $|1\rangle \leftrightarrow |2\rangle$, a coupling field on transition $|2\rangle \leftrightarrow |3\rangle$, and a microwave field on transition $|3\rangle \leftrightarrow |4\rangle$. Two atoms in Rydberg states $|3\rangle$ and $|4\rangle$ exhibit also self vdW (V_{33}^s and V_{44}^s) and exchange DD (V_{34}^e) interactions. (b) Schematic of a microwave electrometry realized in cold atoms, where the probe and coupling fields travel along a common z direction whereas the microwave field illuminates the atomic sample transversely. Small gray and large red spheres denote ordinary and Rydberg atoms, respectively, with the blow-up of a composite structure (containing just one Rydberg atom) acting collectively as a SA.

Rabi frequencies are defined as $\Omega_p = E_p \wp_{12}/2\hbar$, $\Omega_c = E_c \wp_{23}/2\hbar$, and $\Omega_m = E_m \wp_{34}/2\hbar$ while relevant detunings refer to $\Delta_p = \omega_p - \omega_{12}$, $\Delta_c = \omega_c - \omega_{23}$, and $\Delta_m = \omega_m - \omega_{34}$ with $\wp_{\mu\nu}$ and $\omega_{\mu\nu}$ being electric dipole moment and resonant frequency, respectively, on transition $|\mu\rangle \leftrightarrow |\nu\rangle$. The coupling field is applied to generate an EIT window for the probe field while the microwave field will result in an AT splitting of the EIT window. Then the distance between two AT peaks may serve as a direct measure of amplitude E_m for the microwave field. Two atoms located at positions \mathbf{r}_j and \mathbf{r}_k , respectively, if excited to $|3\rangle$ and/or $|4\rangle$ taken here as different Rydberg states, will interact through the self vdW potentials $V_{33}^s = C_{33}^s/|\mathbf{r}_j - \mathbf{r}_k|^6$ and $V_{44}^s = C_{44}^s/|\mathbf{r}_j - \mathbf{r}_k|^6$ as well as the exchange DD potential $V_{34}^e = C_{34}^e/|\mathbf{r}_j - \mathbf{r}_k|^3$, with C_{33}^s , C_{44}^s , and C_{34}^e being respective state-dependent coefficients.

With the above considerations, taking the electric-dipole and rotating-wave approximations as usual, we can write down the total Hamiltonian

$$\mathcal{H} = \mathcal{H}_{af} + \mathcal{H}_v, \quad (1)$$

for a sample of \mathcal{N} cold atoms, where the first term

$$\begin{aligned} \mathcal{H}_{af} = & -\hbar \sum_{j=1}^{\mathcal{N}} \{ [\Delta_p |2\rangle\langle 2|_j + (\Delta_p + \Delta_c)|3\rangle\langle 3|_j \\ & + (\Delta_p + \Delta_c + \Delta_m)|4\rangle\langle 4|_j] \\ & - [\Omega_p |2\rangle\langle 1|_j + \Omega_c |3\rangle\langle 2|_j + \Omega_m |4\rangle\langle 3|_j \\ & + \Omega_p^* |1\rangle\langle 2|_j + \Omega_c^* |2\rangle\langle 3|_j + \Omega_m^* |3\rangle\langle 4|_j] \}, \end{aligned} \quad (2)$$

describes atom-field interactions while the second term

$$\begin{aligned} \mathcal{H}_V = \hbar \sum_{k < j}^N & [\mathcal{V}_{33}^s |3\rangle\langle 3|_k \otimes |3\rangle\langle 3|_j + \mathcal{V}_{44}^s |4\rangle\langle 4|_k \otimes |4\rangle\langle 4|_j \\ & + \mathcal{V}_{34}^e (|4\rangle\langle 3|_k \otimes |3\rangle\langle 4|_j + |3\rangle\langle 4|_k \otimes |4\rangle\langle 3|_j)], \end{aligned} \quad (3)$$

describes both vdW and DD interactions. Taking \mathcal{H} with Lindblad superoperator $\mathcal{L}[\rho^j]$ describing relevant dissipation processes into the master equation

$$\frac{\partial}{\partial t} \rho^j = -\frac{i}{\hbar} [\mathcal{H}, \rho^j] + \mathcal{L}[\rho^j], \quad (4)$$

we can try to examine the dynamic evolution of the density operator ρ^j for the j th atom. It is, however, rather difficult or impossible in principle to obtain an exact solution of this many-body problem because the dynamic evolution of a specific ρ^j depends on many other ρ^k through Rydberg interactions. To overcome this difficulty, we can resort to the SA model [47–49] in the spirit of a mean-field approximation as detailed later.

Along this line, we can replace ρ^j with the mean-field operator ρ and \mathcal{H} with the mean-field Hamiltonian

$$\begin{aligned} H = & -\hbar[\Delta_p |2\rangle\langle 2| + (\Delta_p + \Delta_c - s_{33}) |3\rangle\langle 3| \\ & + (\Delta_p + \Delta_c + \Delta_m - s_{44}) |4\rangle\langle 4|] \\ & + \hbar[\Omega_p |2\rangle\langle 1| + \Omega_c |3\rangle\langle 2| + (\Omega_m + e_{43}) |4\rangle\langle 3| \\ & + \Omega_p^* |1\rangle\langle 2| + \Omega_c^* |2\rangle\langle 3| + (\Omega_m^* + e_{34}) |3\rangle\langle 4|], \end{aligned} \quad (5)$$

appropriate for each atom driven by the three fields along with the Lindblad superoperator

$$\begin{aligned} \mathcal{L}[\rho] = & \begin{pmatrix} \Gamma_{21}\rho_{22} & 0 & 0 & 0 \\ 0 & \Gamma_{32}\rho_{33} & 0 & 0 \\ 0 & 0 & \Gamma_{43}\rho_{44} & 0 \\ 0 & 0 & 0 & 0 \end{pmatrix} \\ & + \begin{pmatrix} 0 & -\gamma_{21}\rho_{12} & -\gamma_{31}\rho_{13} & -\gamma_{41}\rho_{14} \\ -\gamma_{21}\rho_{21} & -\Gamma_{21}\rho_{22} & -\gamma_{32}\rho_{23} & -\gamma_{42}\rho_{24} \\ -\gamma_{31}\rho_{31} & -\gamma_{32}\rho_{32} & -\Gamma_{32}\rho_{33} & -\gamma_{43}\rho_{34} \\ -\gamma_{41}\rho_{41} & -\gamma_{42}\rho_{42} & -\gamma_{43}\rho_{43} & -\Gamma_{43}\rho_{44} \end{pmatrix}, \end{aligned} \quad (6)$$

where $\rho_{\mu\nu}^j$ has been replaced by $\rho_{\mu\nu}$ since all atoms exhibit the same behavior in the mean-field sense. In the above, $\Gamma_{\mu\nu}$ refers to the population decay rate from level $|\mu\rangle$ to level $|\nu\rangle$, while $\gamma_{\mu\nu} = \sum_k (\Gamma_{\mu k} + \Gamma_{\nu k})/2$ refers to the decoherence rate between levels $|\mu\rangle$ and $|\nu\rangle$. Moreover, we have used s_{33} and s_{44} to denote the energy shifts of levels $|3\rangle$ and $|4\rangle$ induced by self vdW interactions; $e_{34} = e_{43}^*$ to denote the coupling rates between levels $|3\rangle$ and $|4\rangle$ induced by exchange DD interactions. Strengths of these Rydberg interactions may be determined by a differential

measurement between a pair of lower states and the pair of higher states under consideration.

With $\rho^j \rightarrow \rho$ and $\mathcal{H} \rightarrow H$ in the mean-field sense, it is then straightforward to expand Eq. (4), for the four-level cascade system of cold atoms in Fig. 1(a), into following single-body density matrix equations

$$\begin{aligned} \partial_t \rho_{11} &= \Gamma_{21}\rho_{22} + (i\Omega_p \rho_{12} + \text{h.c.}), \\ \partial_t \rho_{22} &= \Gamma_{32}\rho_{33} - \Gamma_{21}\rho_{22} + (i\Omega_c \rho_{23} - i\Omega_p \rho_{12} + \text{h.c.}), \\ \partial_t \rho_{44} &= -\Gamma_{43}\rho_{44} - (i\Omega'_m \rho_{34} + \text{h.c.}), \\ \partial_t \rho_{12} &= -\gamma'_{21}\rho_{12} + i\Omega_p^*(\rho_{11} - \rho_{22}) + i\Omega_c \rho_{13}, \\ \partial_t \rho_{13} &= -\gamma'_{31}\rho_{13} + i\Omega_c^* \rho_{12} - i\Omega_p^* \rho_{23} + i\Omega'_m \rho_{14}, \\ \partial_t \rho_{14} &= -\gamma'_{41}\rho_{14} - i\Omega_p^* \rho_{24} + i\Omega'_m \rho_{13}, \\ \partial_t \rho_{23} &= -\gamma'_{32}\rho_{23} + i\Omega_c^*(\rho_{22} - \rho_{33}) - i\Omega_p \rho_{13} + i\Omega'_m \rho_{24}, \\ \partial_t \rho_{24} &= -\gamma'_{42}\rho_{24} - i\Omega_c^* \rho_{34} + i\Omega'_m \rho_{23} - i\Omega_p \rho_{14}, \\ \partial_t \rho_{34} &= -\gamma'_{43}\rho_{34} + i\Omega'_m(\rho_{33} - \rho_{44}) - i\Omega_c \rho_{24}, \end{aligned} \quad (7)$$

restricted by $\sum_\mu \rho_{\mu\mu} = 1$ and $\rho_{\mu\nu} = \rho_{\nu\mu}^*$ with “h.c.” representing a Hermitian conjugate and $\gamma'_{ij} = \gamma_{ij} + id_{ij}$ denoting complex decoherence rates. Here, we have redefined $d_{12} = \Delta_p$, $d_{13} = \Delta_c + \Delta_p - s_{33}$, $d_{14} = \Delta_c + \Delta_p + \Delta_m - s_{44}$, $d_{23} = \Delta_c - s_{33}$, $d_{24} = \Delta_c + \Delta_m - s_{44}$, and $d_{34} = \Delta_m + s_{33} - s_{44}$ as relevant detunings including self vdW interactions, while $\Omega'_m = \Omega_m + e_{43}$ as the microwave Rabi frequency including exchange DD interactions.

The key for numerically solving Eq. (7) then rests with calculating energy shifts s_{33} and s_{44} as well as coupling rates $e_{34} = e_{43}^*$ by adopting the mean-field SA model. We first recall the well-known concept of Rydberg blockade, indicating that at most one atom within a blockade sphere of radius $R_b = [C_{33}(\gamma'_{21} + \Delta_c^2)^{1/2}/\Omega_c^2]^{1/6}$ and volume $V_b = (4\pi/3)R_b^3$ in the EIT regime can be excited to each Rydberg state due to vdW interactions. Note also that atomic excitation to intermediate state $|2\rangle$ will be well suppressed in the EIT window due to quantum destructive interference. Hence, it is appropriate to treat all $n_{\text{SA}} = N_{\text{at}} V_b$ atoms inside this blockade sphere collectively as a SA containing at most one Rydberg excitation with N_{at} being the atomic density. In particular, the zero- and first-order collective states are given by [47–49]

$$\begin{aligned} |1_{\text{SA}}\rangle &= |1_1, 1_2, \dots, 1_j, \dots, 1_{n_{\text{SA}}}\rangle, \\ |2_{\text{SA}}\rangle &= \frac{1}{\sqrt{n_{\text{SA}}}} \sum_{j=1}^{n_{\text{SA}}} |1_1, 1_2, \dots, 2_j, \dots, 1_{n_{\text{SA}}}\rangle, \\ |3_{\text{SA}}\rangle &= \frac{1}{\sqrt{n_{\text{SA}}}} \sum_{j=1}^{n_{\text{SA}}} |1_1, 1_2, \dots, 3_j, \dots, 1_{n_{\text{SA}}}\rangle, \\ |4_{\text{SA}}\rangle &= \frac{1}{\sqrt{n_{\text{SA}}}} \sum_{j=1}^{n_{\text{SA}}} |1_1, 1_2, \dots, 4_j, \dots, 1_{n_{\text{SA}}}\rangle, \end{aligned} \quad (8)$$

while the second- and higher-order collective states can be safely neglected. We then introduce the SA projection (transition) operators $\hat{\Sigma}_{\mu\nu} = |\mu_{\text{SA}}\rangle\langle\nu_{\text{SA}}|$ with $\mu_{\text{SA}} = \nu_{\text{SA}}$ ($\mu_{\text{SA}} \neq \nu_{\text{SA}}$), and use their mean values $\Sigma_{\mu\nu}$ to substitute $\rho_{\mu\nu}$ in Eq. (7) after replacing Ω_p with $\sqrt{n_{\text{SA}}\Omega_p}$ to account for collective enhancement and disregarding Rydberg interactions between different SAs.

In the limit of a weak probe, up to the first-order perturbative expansion, the set of dynamic equations on SA density-matrix elements $\Sigma_{\mu\nu}$ can be solved to yield

$$\begin{aligned}\Sigma_{13} &= \Omega_p\Omega_c(\Delta_p + \Delta_c)\sqrt{n_{\text{SA}}}\Sigma_{11}/A, \\ \Sigma_{14} &= \Omega_p\Omega_c\Omega_m\sqrt{n_{\text{SA}}}\Sigma_{11}/A,\end{aligned}\quad (9)$$

in the case of $\Delta_m = 0$ and $\Gamma_{43} \simeq \Gamma_{32} \rightarrow 0$ by assuming $\Sigma_{22} \ll \Sigma_{33,44} \ll \Sigma_{11}$ in the EIT regime [47–49]. Here we have also set $A = (\Delta_c + \Delta_p)[(\Delta_p - i\gamma_{21})(\Delta_c + \Delta_p) - \Omega_c^2] - (\Delta_p - i\gamma_{21})\Omega_m^2$ for convenience. Proceeding with $\Sigma_{33} = \Sigma_{31}\Sigma_{13}$, $\Sigma_{44} = \Sigma_{41}\Sigma_{14}$, and $\Sigma_{34} = \Sigma_{31}\Sigma_{14}$,

we finally arrive at the following expressions:

$$\begin{aligned}\Sigma_{33} &= \frac{n_{\text{SA}}\Omega_p^2\Omega_c^2(\Delta_c + \Delta_p)^2}{|A|^2 + n_{\text{SA}}\Omega_p^2\Omega_c^2[(\Delta_c + \Delta_p)^2 + \Omega_m^2]}, \\ \Sigma_{44} &= \frac{n_{\text{SA}}\Omega_p^2\Omega_c^2\Omega_m^2}{|A|^2 + n_{\text{SA}}\Omega_p^2\Omega_c^2[(\Delta_c + \Delta_p)^2 + \Omega_m^2]}, \\ \Sigma_{34} &= \frac{n_{\text{SA}}\Omega_p^2\Omega_c^2\Omega_m(\Delta_c + \Delta_p)}{|A|^2 + n_{\text{SA}}\Omega_p^2\Omega_c^2[(\Delta_c + \Delta_p)^2 + \Omega_m^2]},\end{aligned}\quad (10)$$

restricted by $\Sigma_{11} + \Sigma_{33} + \Sigma_{44} = 1$ and $\Sigma_{\mu\nu} = \Sigma_{\nu\mu}^*$. Equations (10) allow us to evaluate the total Rydberg excitation in our atomic sample through $N_{\text{at}}\rho_{33} \approx N_{\text{SA}}\Sigma_{33}$, $N_{\text{at}}\rho_{44} \approx N_{\text{SA}}\Sigma_{44}$, and $N_{\text{at}}\rho_{34} \approx N_{\text{SA}}\Sigma_{34}$ with $N_{\text{SA}} = V_b^{-1}$ being the SA density. Here we have considered that the atomic sample is homogeneously illuminated by all three fields so that $\rho_{\mu\nu}$ and $\Sigma_{\mu\nu}$ are space independent in a good approximation. In this regard, energy shifts s_{33} and s_{44} as well as coupling rates $e_{34} = e_{43}^*$ of each atom interacting with its neighboring atoms can be calculated through the spatial integrations [50,51]

$$\begin{aligned}s_{33} &\equiv \int d^3\mathbf{r}'\mathcal{V}_{33}^s(\mathbf{r} - \mathbf{r}')N_{\text{at}}\rho_{33}(\mathbf{r}') \approx 2\pi \int_0^\pi \sin\theta d\theta \int_R^{r_\theta} dr \frac{C_{33}^s}{r^4} N_{\text{SA}}\Sigma_{33} \approx \frac{4\pi}{3}N_{\text{at}}C_{33}^s N_{\text{SA}}\Sigma_{33}, \\ s_{44} &\equiv \int d^3\mathbf{r}'\mathcal{V}_{44}^s(\mathbf{r} - \mathbf{r}')N_{\text{at}}\rho_{44}(\mathbf{r}') \approx 2\pi \int_0^\pi \sin\theta d\theta \int_R^{r_\theta} dr \frac{C_{44}^s}{r^4} N_{\text{SA}}\Sigma_{44} \approx \frac{4\pi}{3}N_{\text{at}}C_{44}^s N_{\text{SA}}\Sigma_{44}, \\ e_{34} &\equiv \int d^3\mathbf{r}'\mathcal{V}_{34}^e(\mathbf{r} - \mathbf{r}')N_{\text{at}}\rho_{34}(\mathbf{r}') \approx 2\pi \int_0^\pi \sin\theta d\theta \int_R^{r_\theta} dr \frac{C_{34}^e}{r} N_{\text{SA}}\Sigma_{34} \approx 4\pi f(R, r_p)C_{34}^e N_{\text{SA}}\Sigma_{34},\end{aligned}\quad (11)$$

where $f(R, r_p) = \int_0^{\pi/2} \ln(R/r_\theta) \sin\theta d\theta$ is a dimensionless constant, $R = N_{\text{at}}^{-1/3}$ refers to the interatomic distance, while $r_\theta = r_p/\sin\theta$ denotes the distance from the axis to the surface of a cylindrical atomic sample with r_p being the beam radius of a probe field.

With s_{33} , s_{44} , and $e_{34} = e_{43}^*$ in hand, it is easy to solve Eq. (7) in the steady state by taking $\partial_t\rho_{\mu\nu} = 0$ so that we can attain the complex probe susceptibility (proportional to atomic coherence ρ_{21}) as given below

$$\chi_p = \frac{N_{\text{at}}\Omega_{12}^2}{\hbar\epsilon\Omega_p}\rho_{12}. \quad (12)$$

According to the Beer-Lambert law, we can further write down the transmissivity for a probe field passing through a sample of length L as shown in Fig. 1(b)

$$T_p = \exp[-k_p \text{Im}(\chi_p)L], \quad (13)$$

where $k_p = \omega_p/c = 2\pi/\lambda_p$ refers to the vacuum wave vector with λ_p being the probe wavelength.

III. RESULTS AND DISCUSSION

In this section, we make numerical calculations to investigate the microwave electrometry using a many-body system of cold Rydberg atoms in the presence of self vdW and exchange DD interactions. To be more specific, we take $|5S_{1/2}, F=1\rangle$, $|5P_{3/2}, F=2\rangle$, $|60S_{1/2}\rangle$, and $|61P_{1/2}\rangle$ of ^{87}Rb atoms as the four levels in Fig. 1(b) from bottom to top in order. Then, we have the population decay rates [52] $\Gamma_{21} = 2\pi \times 6.0$ MHz, $\Gamma_{32} = 2\pi \times 0.69$ kHz, and $\Gamma_{43} = 2\pi \times 0.30$ kHz as well as the Rydberg interaction coefficients [53–55] $C_{33}^s = 2\pi \times 135$ GHz μm^6 , $C_{44}^s = 2\pi \times 3.15$ GHz μm^6 , and $C_{34}^e = 2\pi \times 40.0$ MHz μm^3 . Moreover, we choose to consider a cylindrical sample of length $L = 1.5$ cm, radius $r_p = 0.25$ mm, and density $N_{\text{at}}/N_0 \in$

[0.1, 2.0] with $N_0 = 1.0 \times 10^{10} \text{ cm}^{-3}$, which promises high probe transmission in two split EIT windows, on one hand, and yields vanishing or very weak Rydberg interactions, on the other hand. In this case, our Rydberg blockade assumption due to self vdW interactions between two atoms in the same Rydberg state holds true because the interatomic distance $R \in \{10, 3.68\} \mu\text{m}$ is obviously larger than the Le Roy radius $r_{\text{LR}} = 1.1 \mu\text{m}$ and the vdW distance $d_{\text{vdW}} = 2.38 \mu\text{m}$ for both Rydberg states [53]. Hence, in line with Ref. [47], it is viable to neglect in our atomic sample unexpected broadening or decoherence effects observed for dense samples [50,56] of 2 or 3 orders larger densities. Of course, a high Rydberg state (e.g., with $n = 60$ considered here) against a low Rydberg state (e.g., with $n = 20 \sim 30$ in the past works) may compensate to a certain extent the big difference in atomic density since Rydberg interactions typically scale with n^{11} . Moreover, we note that two atoms in different Rydberg states always exhibit exchange DD interactions [55,57] because the (resonant) exchange transition does not involve a perturbative correction.

First, we examine the influence of Rydberg interactions on probe transmission in Fig. 2 for fixed microwave and

probe Rabi frequencies by properly varying atomic density. Figure 2(a) shows that, for $N_{\text{at}} = N_0$, two symmetric EIT peaks appear at $\Delta_c^{\pm} = \pm\Omega_m$ due to AT splitting when Rydberg interactions are purposely discarded, but shift slightly rightward to different extents when Rydberg interactions are correctly included. This indicates, Rydberg interactions are significant and result in a nonlinear dependence of $\Delta_f = \Delta_c^+ - \Delta_c^-$ on Ω_m , hence an inaccurate estimation on the microwave field amplitude. Similar plots are given in Fig. 2(b) for $N_{\text{at}} = N_0$, $0.5N_0$, and $0.1N_0$ yet without changing other parameters in the presence of Rydberg interactions. We can see that the two EIT peaks become more and more symmetric by moving leftward and finally stop at $\Delta_c^{\pm} = \pm\Omega_m$ as N_0 continuously decreases to yield gradually negligible Rydberg interactions. It is also clear that the two EIT peaks become broader and broader as N_0 continuously decreases to yield gradually reduced optical depths. The above results can be well understood by illustrating two prominent Rydberg interactions in Figs. 2(c) and 2(d), from which we observe that $|s_{33}| (\gg |s_{44}|)$ due to $C_{33}^s/C_{44}^s \simeq 43$ and $\Sigma_{33} \geq \Sigma_{44}$) is comparable to Ω_m for $N_{\text{at}} = N_0$, but becomes negligible for $N_{\text{at}} = 0.1N_0$; $e_{34} = e_{43}$ is negative for $\Delta_c < 0$ but positive for $\Delta_c > 0$,

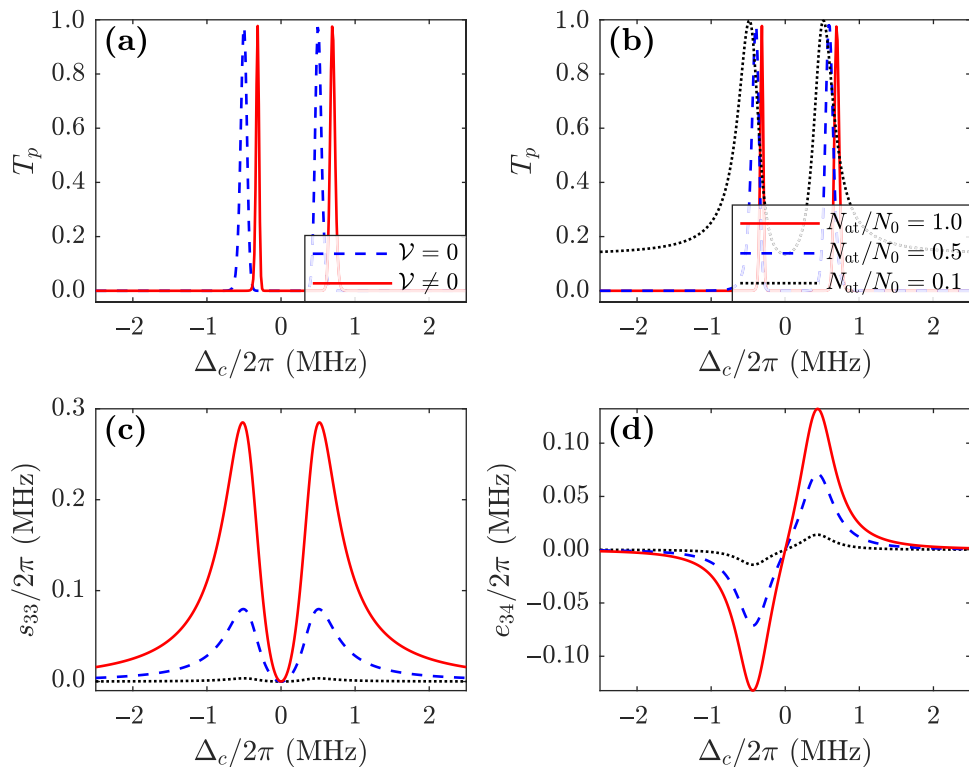


FIG. 2. (a) Probe transmission against coupling detuning in the presence (red solid) or absence (blue dashed) of vdw and DD interactions with $N_{\text{at}}/N_0 = 1.0$. (b) Probe transmission in the presence of vdw and DD interactions, (c) Rydberg shift due to vdw interactions, and (d) Rydberg coupling due to DD interactions against coupling detuning with $N_{\text{at}}/N_0 = 1.0$ (red solid), $N_{\text{at}}/N_0 = 0.5$ (blue dashed), and $N_{\text{at}}/N_0 = 0.1$ (black dotted), respectively. Other parameters are $\Omega_p/2\pi = 0.1 \text{ MHz}$, $\Omega_c/2\pi = 1.25 \text{ MHz}$, $\Omega_m/2\pi = 0.5 \text{ MHz}$, $\Delta_p = \Delta_m = 0$, $\lambda_p = 780 \text{ nm}$, and $\wp_{12} = 1.73 \times 10^{-29} \text{ C m}$ except those specified at the beginning of Sec. III.

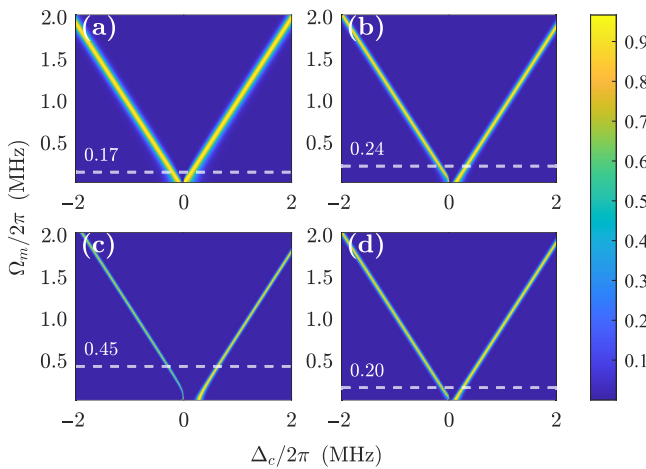


FIG. 3. Probe transmission against microwave Rabi frequency and coupling detuning in the presence of Rydberg interactions with (a) $N_{\text{at}}/N_0 = 0.5$ and $\Omega_p/2\pi = 0.05$ MHz; (b) $N_{\text{at}}/N_0 = 1.0$ and $\Omega_p/2\pi = 0.05$ MHz; (c) $N_{\text{at}}/N_0 = 2.0$ and $\Omega_p/2\pi = 0.05$ MHz; (d) $N_{\text{at}}/N_0 = 2.0$ and $\Omega_p/2\pi = 0.025$ MHz. White dashed lines denote microwave field strengths corresponding to $\Delta\% = 2\%$. Other parameters are the same as in Fig. 2.

thus leading to a Δ_c -dependent effective microwave Rabi frequency $\Omega_m + e_{43}$ so that the two EIT peaks become asymmetric.

Next, we examine the probe transmission against both microwave Rabi frequency Ω_m and coupling detuning Δ_c to gain a more comprehensive insight into the availability of Rydberg microwave metrology. This has been done in Fig. 3 for three different values of not only atomic density N_{at} but also probe Rabi frequency Ω_p by considering that energy shift s_{33} and coupling rate e_{34} depend on Ω_p through SA Rydberg population Σ_{33} and coherence Σ_{34} , respectively. Figures 3(a)–3(c) show that the linear regime characterized by two symmetric EIT peaks appropriate for an accurate microwave metrology reduces evidently as N_{at} gradually increases for a fixed Ω_p . That is, the boundary of linear and nonlinear regimes (roughly marked by a horizontal white line) slowly moves upward for a denser atomic sample exhibiting stronger vdW and DD interactions. A smaller Ω_p can be adopted, however, to counteract the adverse nonlinear effect resulted from a larger N_0 and thus attain a more extended linear regime, which can be seen by comparing Figs. 3(c) and 3(d). This is because smaller probe Rabi frequencies result in lower Rydberg excitations, hence reduced energy shift s_{33} and coupling rate e_{34} is favorable for the accurate measurement of weaker microwave fields.

To further clarify the joint functions of atomic density N_{at} and probe Rabi frequency Ω_p , we extract the measured values Δf of microwave Rabi frequency from Fig. 3 and compare them with corresponding real values Ω_m in terms

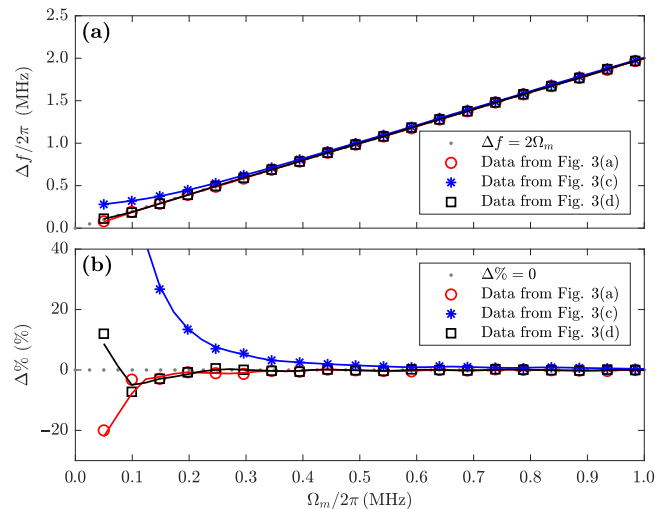


FIG. 4. Measured values of (a) microwave Rabi frequency and (b) their percent differences against real values of microwave Rabi frequency with $N_{\text{at}}/N_0 = 0.5$ and $\Omega_p/2\pi = 0.05$ MHz (red circle); $N_{\text{at}}/N_0 = 2.0$ and $\Omega_p/2\pi = 0.05$ MHz (blue star); $N_{\text{at}}/N_0 = 2.0$ and $\Omega_p/2\pi = 0.025$ MHz (black square). Other parameters are the same as in Fig. 2.

of the percent difference defined as

$$\Delta\% = \frac{\Delta f - 2\Omega_m}{2\Omega_m} \times 100\%. \quad (14)$$

Numerical results are illustrated in Fig. 4 for a few combinations of N_{at} and Ω_p . It is clear that, for $N_{\text{at}}/N_0 = 0.5$ and $\Omega_p = 2\pi \times 0.05$ MHz, Δf deviates evidently from $2\Omega_m$ so that we observe a significant $\Delta\%$ in the nonlinear regime referring to a relatively weak microwave field ($\Omega_m \lesssim 2\pi \times 0.2$ MHz), but coincides well with $2\Omega_m$ so that we observe a vanishing $\Delta\%$ in the linear regime referring to a relatively strong microwave field ($\Omega_m \gtrsim 2\pi \times 0.2$ MHz). The evident deviation of Δf from $2\Omega_m$, hence $\Delta\%$ from vanishing, occurs however for a stronger microwave field ($\Omega_m \gtrsim 2\pi \times 0.5$ MHz) to result in a reduced linear regime as we consider a denser atomic sample with $N_{\text{at}}/N_0 = 2.0$ while keeping $\Omega_p = 2\pi \times 0.05$ MHz. Fortunately, we can roughly recover the original linear regime (i.e., attain a vanishing $\Delta\%$ for $\Omega_m \gtrsim 2\pi \times 0.2$ MHz again) by simply applying a weaker probe field with $\Omega_p = 2\pi \times 0.025$ MHz. Above discussions indicate that N_{at} and Ω_p jointly determine the strengths of nonlocal Rydberg interactions, thus the available linear regime for accurate microwave measurements.

Then, we plot in Fig. 5 several critical lines with respect to N_{at} and Ω_p , below which Δf differs from Ω_m by $|\Delta\%| \leq 2\%$ for a microwave field not weaker than that used in the corresponding calculation. Figure 5(a) shows that a critical line will move upward (i.e., toward both larger N_{at} and larger Ω_p) to result in an extended linear regime as it is calculated with

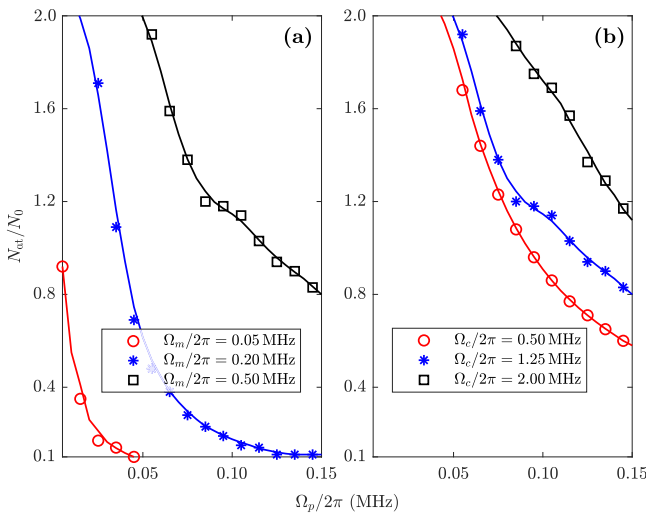


FIG. 5. Critical lines referring to $|\Delta\%| = 2\%$ as joint variations of probe Rabi frequency and atomic density with (a) $\Omega_m/2\pi = 0.05$ MHz (red circle), 0.2 MHz (blue star), and 0.5 MHz (black square); (b) $\Omega_c/2\pi = 0.5$ MHz (red circle), 1.25 MHz (blue star), and 2.0 MHz (black square). Other parameters are the same as in Fig. 2 except $\Omega_c/2\pi = 1.25$ MHz in (a) and $\Omega_m/2\pi = 0.5$ MHz in (b).

a stronger microwave field. This can be understood by analyzing the relationship between Rydberg interactions and microwave intensity. Specifically, diagonalizing the two-level Hamiltonian for Rydberg states $|3\rangle$ and $|4\rangle$ yields its eigenvalues: $E_{\pm} = (s_{33} + s_{44})/2 \pm \sqrt{(2\Omega_m + 2e_{34})^2 + (s_{33} + s_{44})^2}/2$, referring to the modified positions of two EIT peaks. In the case of Ω_m comparable to s_{33} or e_{34} , E_{\pm} are strongly affected by Rydberg interactions, leading thus to a large $|\Delta\%|$. Conversely, when Ω_m is much larger than s_{33} and e_{34} , Rydberg interactions have little effects on E_{\pm} , leading thus to a negligible $|\Delta\%|$. Then, based on the fact that s_{33} and e_{34} are roughly independent of Ω_m in the case of $\Gamma_{43,32} \ll \Omega_m$, an increase of Ω_m will evidently reduce $|\Delta\%|$ and must broaden the available range of N_{at} and Ω_p referring to an invariant $|\Delta\%|$. Note also that N_{at} and Ω_p exhibit an inverse relationship along each critical line because N_{at} must be reduced as Ω_p increases in order to ensure a constant Rydberg excitation $N_{\text{at}}\rho_{33}$, dominant over $N_{\text{at}}\rho_{44}$ since $|s_{33}| \gg |s_{44}|$. Similar results can be found from Fig. 5(b) where a critical line moves upward to yield an extended linear regime as it is calculated with a stronger coupling field. This is because an increase of Ω_c results in a reduction of Rydberg excitation $N_{\text{at}}\rho_{33} \approx N_{\text{SA}}\Sigma_{33} = N_{\text{at}}\Omega_p^2/(\Omega_c^2 + 2n_{\text{SA}}\Omega_p^2)$, leading thus to less SA population Σ_{33} and smaller energy shift s_{33} . That means, we can opt to increase N_{at} or Ω_p so as to maintain a constant $N_{\text{at}}\rho_{33}$ while increasing Ω_c .

With these critical lines, we can determine the minimum detectable microwave electric field E_{\min} against N_{at} for different values of Ω_p and Ω_c as shown in Fig. 6.

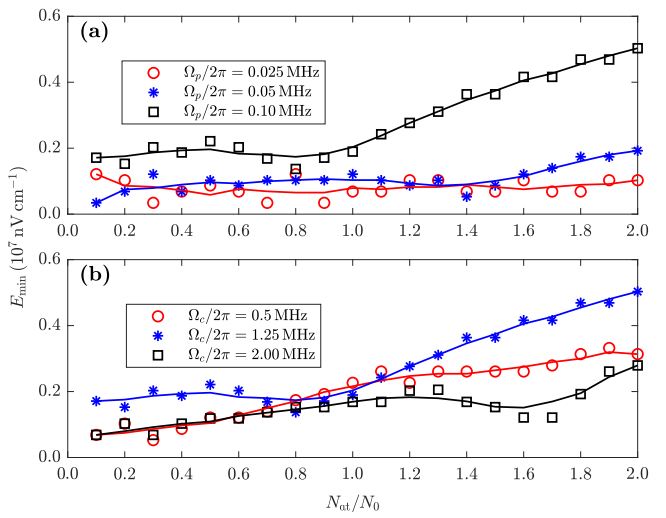


FIG. 6. Minimum detectable electric field determined by critical lines referring to $|\Delta\%| = 2\%$ against atomic density with (a) $\Omega_p/2\pi = 0.025$ MHz (red circle), 0.05 MHz (blue star), and 0.1 MHz (black square); (b) $\Omega_c/2\pi = 0.5$ MHz (red circle), 1.25 MHz (blue star), and 2.0 MHz (black square). Other parameters are the same as in Fig. 2 except $\Omega_c/2\pi = 1.25$ MHz in (a) and $\Omega_p/2\pi = 0.1$ MHz in (b).

It is not difficult to see from Fig. 6(a) that E_{\min} keeps roughly invariant on average for $\Omega_p = 0.025$ MHz, but increases continuously on average for $\Omega_p = 0.05$ MHz and $\Omega_p = 0.1$ MHz, as N_{at} becomes larger and larger. Here we have considered that a microwave field with $\Omega_m < E_{\min}\varrho_{34}/2\hbar$ cannot be accurately measured due to the non-linear dependence of Δf on Ω_m resulted from essential Rydberg interactions. We further find from Fig. 6(b) that E_{\min} slowly increases as N_{at} becomes larger and larger for a fixed Ω_c , but first increases and then decreases as Ω_c becomes larger and larger for a fixed N_{at} , on the whole.

We learn from Fig. 6 that lower atomic densities and weaker probe fields should be chosen to accurately measure weaker microwave fields. This is also restricted by the sensitivity of minimum detectable electric field determined by SQL of shot noises and given by [23,37]

$$S = \frac{E_{\min}}{\sqrt{\text{Hz}}} = \frac{\hbar}{\varrho_{34}\sqrt{N_{\text{eff}}T_2}}, \quad (15)$$

with $T_2 = (\Gamma_{43}^{-1} + \Gamma_{32}^{-1})/2$ and $N_{\text{eff}} = \pi r_p^2 L N_{\text{at}}\rho_{33}$. Now, let us examine the impact of Rydberg interactions on the microwave electrometry from the perspective of sensitivity S . Figure 7 illustrates the variation of sensitivity S with respect to atomic density N_{at} by considering both cases in the absence or presence of Rydberg interactions. We find that, for $N_{\text{at}} \lesssim 0.5N_0$, sensitivity S remains indistinguishable no matter whether Rydberg interactions are included or not and Ω_m is smaller or larger though it rapidly reduces as N_{at} increases. For $0.5N_0 \lesssim N_{\text{at}} \lesssim N_0$,

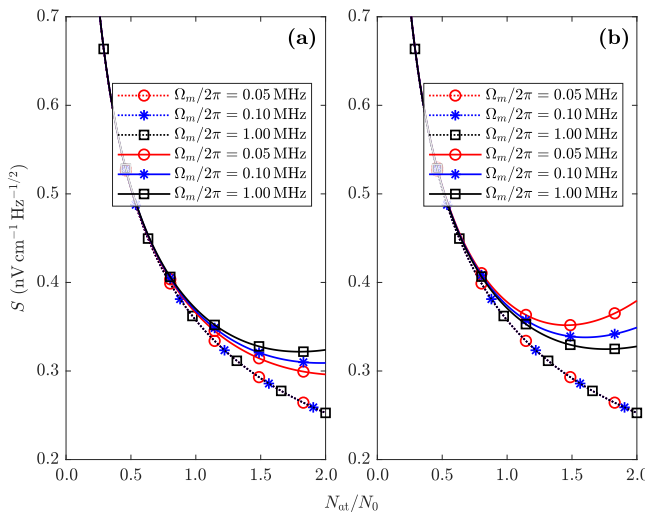


FIG. 7. Sensitivity of minimum detectable electric field against atomic density at (a) $\Delta_c = -\Omega_m/2$; (b) $\Delta_c = \Omega_m/2$. Red-circle, blue-star, and black-square lines refer to $\Omega_m/2\pi = 0.05$ MHz, 0.1 MHz, and 1.0 MHz, respectively. Solid (dotted) lines are attained in the presence (absence) of Rydberg interactions. Other parameters are the same as in Fig. 2 except $\Omega_p/2\pi = 0.07$ MHz and $\Omega_c/2\pi = 1.5$ MHz.

the difference between S attained with Rydberg interactions and that without Rydberg interactions becomes more significant but remains indistinguishable for different values of Ω_m . For $N_{\text{at}} \gtrsim N_0$, S becomes sensitive to Ω_m when Rydberg interactions are considered, though is still independent of Ω_m when Rydberg interactions are absent. Based on these observations, we conclude that by selecting an appropriate N_{at} in a certain range, the measured value of S can be further reduced, thereby improving the precision of microwave-field measurement.

IV. CONCLUSIONS

In summary, we have investigated the effects of weak vdW and DD interactions in a microwave measurement system based on cold Rydberg atoms driven into the EIT regime. Numerical results show that energy shifts due to self vdW interactions and coupling rates due to exchange DD interactions may bring this system into a nonlinear regime where measured values of the microwave Rabi frequency deviate from real ones, which is especially evident for stronger probe fields and denser atomic samples. Hence, we have found critical lines with respect to atomic density and probe Rabi frequency only below which Rydberg interactions can be neglected to make accurate measurement of microwave electric fields. In this regard, the minimum detectable electric field at boundaries of the linear and nonlinear regimes is determined by Rydberg excitations depending on both atomic density and probe Rabi frequency. Moreover, the sensitivity of minimum

detectable electric field is controlled by Rydberg interactions even in the linear regime because they can make the microwave field off resonance by introducing different energy shifts for the two Rydberg states. We hope that our findings could shed light on future works of Rydberg microwave electrometry, e.g., for pursuing an optimal compromise between high precision and high accuracy (requiring more and less Rydberg excitations, respectively) of weaker microwave measurement.

ACKNOWLEDGMENTS

This work is supported by the National Natural Science Foundation of China (Grants No. 12074061 and No. 62375047).

- [1] C. S. Adams, J. D. Pritchard, and J. P. Shaffer, Rydberg atom quantum technologies, *J. Phys. B: At. Mol. Opt. Phys.* **53**, 012002 (2020).
- [2] J. A. Sedlacek, A. Schwettmann, H. Kübler, R. Löw, T. Pfau, and J. P. Shaffer, Microwave electrometry with Rydberg atoms in a vapour cell using bright atomic resonances, *Nat. Phys.* **8**, 819 (2012).
- [3] D. A. Anderson, A. Schwarzkopf, S. A. Miller, N. Thaicharoen, G. Raithel, J. A. Gordon, and C. L. Holloway, Two-photon microwave transitions and strong-field effects in a room-temperature Rydberg-atom gas, *Phys. Rev. A* **90**, 043419 (2014).
- [4] A. Facon, E. K. Dietsche, D. Gross, S. Haroche, J. M. Raimond, M. Brune, and S. Gleyzes, A sensitive electrometer based on a Rydberg atom in a Schrödinger-cat state, *Nature* **535**, 262 (2016).
- [5] K. C. Cox, D. H. Meyer, F. K. Fatemi, and P. D. Kunz, Quantum-limited atomic receiver in the electrically small regime, *Phys. Rev. Lett.* **121**, 110502 (2018).
- [6] M. T. Simons, A. H. Haddab, J. A. Gordon, and C. L. Holloway, A Rydberg atom-based mixer: Measuring the phase of a radio frequency wave, *Appl. Phys. Lett.* **114**, 114101 (2019).
- [7] M. Jing, Y. Hu, J. Ma, H. Zhang, L. Zhang, L. Xiao, and S. Jia, Atomic superheterodyne receiver based on microwave-dressed Rydberg spectroscopy, *Nat. Phys.* **16**, 911 (2020).
- [8] D.-S. Ding, Z.-K. Liu, B.-S. Shi, G.-C. Guo, K. Mølmer, and C. S. Adams, Enhanced metrology at the critical point of a many-body Rydberg atomic system, *Nat. Phys.* **18**, 1447 (2022).
- [9] Z. K. Liu, L. H. Zhang, B. Liu, Z. Y. Zhang, G. C. Guo, D. S. Ding, and B. S. Shi, Deep learning enhanced Rydberg multifrequency microwave recognition, *Nat. Commun.* **13**, 1997 (2022).
- [10] Y. Cai, S. Shi, Y. Zhou, Y. Li, J. Yu, W. Li, and L. Li, High-sensitivity Rydberg-atom-based phase-modulation receiver for frequency-division-multiplexing communication, *Phys. Rev. Appl.* **19**, 044079 (2023).
- [11] D. A. Anderson, S. A. Miller, G. Raithel, J. A. Gordon, M. L. Butler, and C. L. Holloway, Optical measurements of

- strong microwave fields with Rydberg atoms in a vapor cell, *Phys. Rev. Appl.* **5**, 034003 (2016).
- [12] M. T. Simons, J. A. Gordon, C. L. Holloway, D. A. Anderson, S. A. Miller, and G. Raithel, Using frequency detuning to improve the sensitivity of electric field measurements via electromagnetically induced transparency and Autler-Townes splitting in Rydberg atoms, *Appl. Phys. Lett.* **108**, 174101 (2016).
- [13] D. A. Anderson and G. Raithel, Continuous-frequency measurements of high-intensity microwave electric fields with atomic vapor cells, *Appl. Phys. Lett.* **111**, 053504 (2017).
- [14] N. Thaicharoen, K. R. Moore, D. A. Anderson, R. C. Powell, E. Peterson, and G. Raithel, Electromagnetically induced transparency, absorption, and microwave-field sensing in a Rb vapor cell with a three-color all-infrared laser system, *Phys. Rev. A* **100**, 063427 (2019).
- [15] K.-Y. Liao, H.-T. Tu, S.-Z. Yang, C.-J. Chen, X.-H. Liu, J. Liang, X.-D. Zhang, H. Yan, and S.-L. Zhu, Microwave electrometry via electromagnetically induced absorption in cold Rydberg atoms, *Phys. Rev. A* **101**, 053432 (2020).
- [16] F.-D. Jia, X.-B. Liu, J. Mei, Y.-H. Yu, H.-Y. Zhang, Z.-Q. Lin, H.-Y. Dong, J. Zhang, F. Xie, and Z.-P. Zhong, Span shift and extension of quantum microwave electrometry with Rydberg atoms dressed by an auxiliary microwave field, *Phys. Rev. A* **103**, 063113 (2021).
- [17] N. Prajapati, A. K. Robinson, S. Berweger, M. T. Simons, A. B. Artusio-Glimpse, and C. L. Holloway, Enhancement of electromagnetically induced transparency based Rydberg-atom electrometry through population repumping, *Appl. Phys. Lett.* **119**, 214001 (2021).
- [18] A. K. Robinson, A. B. Artusio-Glimpse, M. T. Simons, and C. L. Holloway, Atomic spectra in a six-level scheme for electromagnetically induced transparency and Autler-Townes splitting in Rydberg atoms, *Phys. Rev. A* **103**, 023704 (2021).
- [19] M. T. Simons, A. B. Artusio-Glimpse, C. L. Holloway, E. Imhof, S. R. Jefferts, R. Wyllie, B. C. Sawyer, and T. G. Walker, Continuous radio-frequency electric-field detection through adjacent Rydberg resonance tuning, *Phys. Rev. A* **104**, 032824 (2021).
- [20] C. L. Holloway, N. Prajapati, A. B. Artusio-Glimpse, S. Berweger, M. T. Simons, Y. Kasahara, A. Alú, and R. W. Ziolkowski, Rydberg atom-based field sensing enhancement using a split-ring resonator, *Appl. Phys. Lett.* **120**, 204001 (2022).
- [21] Y.-L. Zhou, D. Yan, and W. Li, Rydberg electromagnetically induced transparency and absorption of strontium triplet states in a weak microwave field, *Phys. Rev. A* **105**, 053714 (2022).
- [22] Y. Cui, F.-D. Jia, J.-H. Hao, Y.-H. Wang, F. Zhou, X.-B. Liu, Y.-H. Yu, J. Mei, J.-H. Bai, Y.-Y. Bao, D. Hu, Y. Wang, Y. Liu, J. Zhang, F. Xie, and Z.-P. Zhong, Extending bandwidth sensitivity of Rydberg-atom-based microwave electrometry using an auxiliary microwave field, *Phys. Rev. A* **107**, 043102 (2023).
- [23] J. Kitching, S. Knappe, and E. A. Donley, Atomic sensors - a review, *IEEE Sens. J.* **11**, 1749 (2011).
- [24] C. L. Degen, F. Reinhard, and P. Cappellaro, Quantum sensing, *Rev. Mod. Phys.* **89**, 035002 (2017).
- [25] D. A. Anderson, R. E. Sapiro, and G. Raithel, Rydberg atoms for radio-frequency communications and sensing: Atomic receivers for pulsed rf field and phase detection, *IEEE Aerosp. Electron. Syst. Mag.* **35**, 48 (2020).
- [26] S. M. Bohaichuk, D. Booth, K. Nickerson, H. Tai, and J. P. Shaffer, Origins of Rydberg-atom electrometer transient response and its impact on radio-frequency pulse sensing, *Phys. Rev. Appl.* **18**, 034030 (2022).
- [27] M. Noaman, D. W. Booth, and J. P. Shaffer, Rydberg-atom sensors in bichromatic radio-frequency fields, *Phys. Rev. Appl.* **20**, 024068 (2023).
- [28] H. Q. Fan, S. Kumar, R. Daschner, H. Kubler, and J. P. Shaffer, Subwavelength microwave electric-field imaging using Rydberg atoms inside atomic vapor cells, *Opt. Lett.* **39**, 3030 (2014).
- [29] C. L. Holloway, J. A. Gordon, A. Schwarzkopf, D. A. Anderson, S. A. Miller, N. Thaicharoen, and G. Raithel, Sub-wavelength imaging and field mapping via electromagnetically induced transparency and Autler-Townes splitting in Rydberg atoms, *Appl. Phys. Lett.* **104**, 244102 (2014).
- [30] C. L. Holloway, M. T. Simons, J. A. Gordon, P. F. Wilson, C. M. Cooke, D. A. Anderson, and G. Raithel, Atom-based rf electric field metrology: From self-calibrated measurements to subwavelength and near-field imaging, *IEEE Trans. Electromagn. Compat.* **59**, 717 (2017).
- [31] C. G. Wade, N. Šibalić, N. R. de Melo, J. M. Kondo, C. S. Adams, and K. J. Weatherill, Real-time near-field terahertz imaging with atomic optical fluorescence, *Nat. Photonics* **11**, 40 (2016).
- [32] L. A. Downes, A. R. MacKellar, D. J. Whiting, C. Bourgenot, C. S. Adams, and K. J. Weatherill, Full-field terahertz imaging at kilohertz frame rates using atomic vapor, *Phy. Rev. X* **10**, 011027 (2020).
- [33] M. Fleischhauer, A. Imamoglu, and J. P. Marangos, Electromagnetically induced transparency: Optics in coherent media, *Rev. Mod. Phys.* **77**, 633 (2005).
- [34] B. K. Teo, D. Feldbaum, T. Cubel, J. R. Guest, P. R. Berman, and G. Raithel, Autler-Townes spectroscopy of the $5S_1/2$ - $5P_3/2$ - $44D$ cascade of cold 8S Rb atoms, *Phys. Rev. A* **68**, 053407 (2003).
- [35] P. M. Anisimov, J. P. Dowling, and B. C. Sanders, Objectively discerning Autler-Townes splitting from electromagnetically induced transparency, *Phys. Rev. Lett.* **107**, 163604 (2011).
- [36] C. L. Holloway, J. A. Gordon, S. Jefferts, A. Schwarzkopf, D. A. Anderson, S. A. Miller, N. Thaicharoen, and G. Raithel, Broadband Rydberg atom-based electric-field probe for SI-traceable, self-calibrated measurements, *IEEE Trans. Antennas Propag.* **62**, 6169 (2014).
- [37] H. Fan, S. Kumar, J. Sedlacek, H. Kübler, S. Karimkashi, and J. P. Shaffer, Atom based rf electric field sensing, *J. Phys. B: At. Mol. Opt. Phys.* **48**, 202001 (2015).
- [38] F. Zhou, F. Jia, X. Liu, Y. Yu, J. Mei, J. Zhang, F. Xie, and Z. Zhong, Improving the spectral resolution and measurement range of quantum microwave electrometry by cold Rydberg atoms, *J. Phys. B: At. Mol. Opt. Phys.* **56**, 025501 (2023).
- [39] S. Whitlock, Many atoms make sensors better, *Nat. Phys.* **18**, 1391 (2022).

- [40] D. Maxwell, D. J. Szwier, D. Paredes-Barato, H. Busche, J. D. Pritchard, A. Gauguet, K. J. Weatherill, M. P. A. Jones, and C. S. Adams, Storage and control of optical photons using Rydberg polaritons, *Phys. Rev. Lett.* **110**, 103001 (2013).
- [41] L. Ma, X. Lei, J. Yan, R. Li, T. Chai, Z. Yan, X. Jia, C. Xie, and K. Peng, High-performance cavity-enhanced quantum memory with warm atomic cell, *Nat. Commun.* **13**, 2368 (2022).
- [42] S. J. Evered, D. Bluvstein, M. Kalinowski, S. Ebadi, T. Manovitz, H. Zhou, S. H. Li, A. A. Geim, T. T. Wang, N. Maskara, H. Levine, G. Semeghini, M. Greiner, V. Vuletić, and M. D. Lukin, High-fidelity parallel entangling gates on a neutral-atom quantum computer, *Nature* **622**, 268 (2023).
- [43] D. Bluvstein, *et al.*, Logical quantum processor based on reconfigurable atom arrays, *Nature* **626**, 58 (2024).
- [44] S. Ebadi, T. T. Wang, H. Levine, A. Keesling, G. Semeghini, A. Omran, D. Bluvstein, R. Samajdar, H. Pichler, W. W. Ho, S. Choi, S. Sachdev, M. Greiner, V. Vuletić, and M. D. Lukin, Quantum phases of matter on a 256-atom programmable quantum simulator, *Nature* **595**, 227 (2021).
- [45] P. Scholl, M. Schuler, H. J. Williams, A. A. Eberharter, D. Barredo, K. N. Schymik, V. Lienhard, L. P. Henry, T. C. Lang, T. Lahaye, A. M. Lauchli, and A. Browaeys, Quantum simulation of 2D antiferromagnets with hundreds of Rydberg atoms, *Nature* **595**, 233 (2021).
- [46] S. Kumar, H. Fan, H. Kübler, J. Sheng, and J. P. Shaffer, Atom-based sensing of weak radio frequency electric fields using homodyne readout, *Sci. Rep.* **7**, 42981 (2017).
- [47] D. Petrosyan, J. Otterbach, and M. Fleischhauer, Electromagnetically induced transparency with Rydberg atoms, *Phys. Rev. Lett.* **107**, 213601 (2011).
- [48] D. Yan, Y.-M. Liu, Q.-Q. Bao, C.-B. Fu, and J.-H. Wu, Electromagnetically induced transparency in an inverted system of interacting cold atoms, *Phys. Rev. A* **86**, 023828 (2012).
- [49] Y.-M. Liu, X.-D. Tian, D. Yan, Y. Zhang, C.-L. Cui, and J.-H. Wu, Nonlinear modifications of photon correlations via controlled single and double Rydberg blockade, *Phys. Rev. A* **91**, 043802 (2015).
- [50] B. J. DeSalvo, J. A. Aman, C. Gaul, T. Pohl, S. Yoshida, J. Burgdörfer, K. R. A. Hazzard, F. B. Dunning, and T. C. Killian, Rydberg-blockade effects in Autler-Townes spectra of ultracold strontium, *Phys. Rev. A* **93**, 022709 (2016).
- [51] J. Han, T. Vogt, and W. Li, Spectral shift and dephasing of electromagnetically induced transparency in an interacting Rydberg gas, *Phys. Rev. A* **94**, 043806 (2016).
- [52] Daniel A. Steck, Rubidium 87 D Line Data, available online at <http://steck.us/alkalidata> (revision 2.3.2, 10 September 2023).
- [53] N. Šibalić, J. Pritchard, C. Adams, and K. Weatherill, ARC: An open-source library for calculating properties of alkali Rydberg atoms, *Comput. Phys. Commun.* **220**, 319 (2017).
- [54] S. Weber, C. Tresp, H. Menke, A. Urvoy, O. Firstenberg, H. P. Büchler, and S. Hofferberth, Calculation of Rydberg interaction potentials, *J. Phys. B: At. Mol. Opt. Phys.* **50**, 133001 (2017).
- [55] Z. Zeybek, R. Mukherjee, and P. Schmelcher, Quantum phases from competing van der Waals and dipole-dipole interactions of Rydberg atoms, *Phys. Rev. Lett.* **131**, 203003 (2023).
- [56] E. A. Goldschmidt, T. Boulier, R. C. Brown, S. B. Koller, J. T. Young, A. V. Gorshkov, S. L. Rolston, and J. V. Porto, Anomalous broadening in driven dissipative Rydberg systems, *Phys. Rev. Lett.* **116**, 113001 (2016).
- [57] D. Petrosyan and K. Mølmer, Binding potentials and interaction gates between microwave-dressed Rydberg atoms, *Phys. Rev. Lett.* **113**, 123003 (2014).